NASA/TM—2001-210669

Inter-Cusp Ion and Electron Transport in a NSTAR-Derivative Ion Thruster

John E. Foster
Glenn Research Center, Cleveland, Ohio

National Aeronautics and
Space Administration

Glenn Research Center

March 2001

Available from

NASA Center for Aerospace Information
7121 Standard Drive
Hanover, MD 21076
Price Code: A03

National Technical Information Service
5285 Port Royal Road
Springfield, VA 22100
Price Code: A03

Available electronically at http://gltrs.grc.nasa.gov/GLTRS

INTER-CUSP ION AND ELECTRON TRANSPORT IN A NSTAR-DERIVATIVE ION THRUSTER

John E. Foster
National Aeronautics and Space Administration
Glenn Research Center
Cleveland, Ohio 44135

SUMMARY

Diffusion of electrons and ions to anode surfaces between the magnetic cusps of a NASA Solar Electric Propulsion Technology Application Readiness ion thruster has been characterized. Ion flux measurements were made at the anode and at the screen grid electrode. The measurements indicated that the average ion current density at the anode and at the screen grid were approximately equal. Additionally, it was found that the electron flux to the anode between cusps is best described by the classical cross-field diffusion coefficient.

NOMENCLATURE

B	transverse magnetic field
d	plasma sheath thickness
D_e	electron diffusion coefficient, B = 0
$D_\perp$	electron cross-field diffusion coefficient
E_s	Sheath electric field
e	elementary charge of an electron
J_e	electron cross-field current density
$J_{scrn.grd}$	ion current density at the screen grid
$J_{Wall\ B}$	ion current density at wall probe B
K	Boltzmann's constant
M	mass of an electron
n_e	electron number density
r	radial displacement
T_{eA}	electron temperature at probe A
T_{eB}	electron temperature at probe B
T_e	electron temperature
ΔV	voltage drop across plasma sheath
μ	electron mobility
ν_e	total electron collision frequency
w	electron cyclotron frequency

INTRODUCTION

Controlling ion and electron transport to discharge chamber surfaces is a key aspect of ion thruster design (refs. 1 and 2). Indeed, at a given thruster power, performance can be optimized by maximizing the fraction of discharge ions that reach the ion extraction optics. Maximizing the extracted ion fraction can be achieved by minimizing ion losses to the anode. Reducing the flow of ions to surfaces other than the extraction optics using a magnetic field is usually not practical due to the very strong field strengths required to magnetize ion motion. Instead, thruster magnetic circuits, such as the ring cusp, utilize magnetic field geometries that contain electrons in a manner such that the discharge produced is located just upstream of the ion optics (ref. 3). The close proximity of discharge to the collection optics increases the likelihood that an ion generated in this volume will be extracted.

It has been suggested that many ion thruster discharge chamber configurations operate with preferential ion flow to the ion optics (ref. 1). Whether or not the ring cusp magnetic circuit of the NASA Solar Electric Propulsion Technology Application Readiness (NSTAR) (ref. 4) ion thruster investigated in this work can affect ion motion to the

anode and thereby improve ion flow to the optics is a question that is addressed in this work. An understanding of the nature of ion flow from the discharge to the ion optics can be used as a guide in both optimizing the performance of this thruster and also increasing the thruster's power range.

Unlike ion motion, electron motion is severely affected by the presence of the inter-cusp magnetic field. In this work, electron diffusion to the anode surfaces between the magnetic cusps was also studied. The magnetic field between cusps provides a fairly high impedance path for electron flow to the anode, thereby reducing electron losses to the anode. The character of the cross-field electron diffusion coefficient is a measure of this impedance. A large cross-field diffusion coefficient would lead to a lower discharge voltage and consequently, a reduction in the bulk plasma ionization rate. Previous investigations of electron diffusion between cusps have assumed anomalous Bohm diffusion (ref. 5). In this work, the nature of the cross-field electron diffusion coefficient in a NSTAR-derivative ion thruster is determined.

EXPERIMENTAL APPARATUS

The ion thruster used in this investigation was mechanically identical to the NSTAR thruster (ref. 4). A schematic of the ion thruster and internal discharge chamber wall probes is illustrated in figure 1. A screen grid and accelerator grid comprised the high-voltage ion extraction optics. The voltages at the screen and accelerator grid electrodes ranged from 650 to 1500 V and −250 to −180 V, respectively, as thruster input power varied from 0.5 to 4.6 kW. It should be noted that for this engine, the ratio of peak to average ion beam current density as measured in the plume varied from 0.45 to 0.55 over the range of conditions investigated. Additional details regarding the 30-cm engine, the power console, and the propellant feed system can be found elsewhere (refs. 4, 6, and 7). As can be seen in figure 1, the aluminum discharge chamber was conical with a downstream cylindrical section. The magnetic circuit consisted of only three permanent magnet rings: (1) the cathode ring, located at the back-plate of the conical section; (2) the cylindrical section ring, located at the junction between the cylindrical section and the conical section; and (3) the downstream ring, located at the most downstream flange of the cylindrical section. For these investigations, xenon propellant is used.

The planar molybdenum wall probes used in this investigation each measured 6.4 mm in diameter. The wall probes were flush mounted with the surface of the anode at positions indicated in figure 1. The probes were designated according to the letters as indicated in figure 1. Wall probe A was located near the midpoint between the cathode and cylinder magnetic cusps and wall probe B was located near the midpoint between the cylinder and pole piece magnetic cusps. The transverse magnetic field component across the surface of wall probes A and B was approximately 0.0021 and 0.0023 T, respectively. The probes were electrically isolated from the anode wall and were held in place using modified compression fittings. The wall probes were biased relative to cathode potential using a variable DC voltage source to obtain Langmuir current-voltage characteristics from which plasma density and electron temperature were calculated. In order to obtain the average ion current density at the screen grid, the grid was negatively biased −25 V with respect to the discharge cathode. For this investigation, thruster discharge power ranged between 120 and 465 W, which corresponded to a total thruster input power between 0.5 and 4.6 kW.

RESULTS AND DISCUSSION

Background

Between the cusps, the magnetic field lines run parallel to the surface of the anode. This field limits the cross-field diffusion of electrons to the anode surface. Figures 2(a) and (b) illustrate the variation in the normalized transverse magnetic field component at the anode as a function of position relative to the magnetic cusps. The normalized transverse field in the conical section of the discharge chamber is normalized to the transverse field intensity near the cathode cusp. For reference, the transverse magnetic field intensity at the anode one centimeter from the cathode ring magnetic cusp was 0.053 T. The normalized transverse field in the cylindrical section is normalized to the transverse field intensity near the cylindrical section magnetic cusp. The magnetic cusps are located at positions 0 and 18-cm of figure 2(a) and positions 0- and 12-cm of figure 2(b). Along the anode, at distances greater than 2.5-cm away from the magnetic cusps, the transverse field does not vary appreciably. As can be seen in the figures, an appreciable portion of the anode surface lie in these regions of relatively constant transverse magnetic field. Indeed, over 70 percent of the anode's surface area lies in these regions of relatively constant transverse magnetic

field. The transverse magnetic field component in these regions is less than 20 percent of the transverse component measured near the cusps. Plasma collection at anode surfaces located close to the magnetic cusps is associated with magnetic cusp physics and is not the subject of this investigation.

The focus of this work is to ascertain the effect that the intercusp magnetic field has on ion and electron transport to anode surfaces. Accordingly, this work is divided into two sections: (1) ion transport and (2) electron transport.

Ion Transport

Ion loss to the anode between the magnetic cusps and to the screen grid was determined by biasing wall probes A and B and the screen grid negative of the cathode potential to obtain the ion saturation current density. Figure 3 depicts a schematic of ion losses to bounding discharge chamber surfaces in the cylindrical section. The screen grid, which has a 67 percent open area, is the most downstream boundary of the discharge chamber's cylindrical section. If preferential ion drift to the ion optics occurs in the NSTAR-derivative thruster, then it can be expected that the ion current density measured at the cylindrical section sidewall as measured by wall probe B should be less than the average ion current density measured at the biased screen grid. A plot of the ratio of ion current density measured at the screen grid to the ion current density measured at wall probe B is shown in figure 4. For the discharge powers investigated, the ratio was nearly unity. This result is surprising in that it does not indicate a preferential flow of ions to the optics at any discharge power as has been suggested by an earlier study (ref. 1). It should be pointed out that in the earlier study, the magnetic circuit as well as the anode geometry differed significantly from the NSTAR-derivative ion thruster studied in this present investigation. As determined from measurements presented here, the ion losses to the cylindrical section boundaries and the screen grid are approximately equal. It should be pointed out that such ion flow is consistent with the work of Masek (ref. 8).

Past studies have suggested that the extracted ion beam fraction is considerably larger than that that would be expected from the ratio of screen grid physical open area to total discharge chamber surface area (refs. 1, 9 and 10). This result is attributable in part to an increase in screen grid transparency during high voltage extraction (refs. 8 and 11). The remaining disparity can be addressed through an examination anode wall probe data. Figure 5 illustrates the behavior of the ion saturation current ratio of wall probe B to wall probe A as a function of discharge power. In all cases, the ion current measured at probe B was approximately a factor of 1.55-times larger than that measured at probe A.

If the discharge ions escaping to the ion beam optics and to the cylindrical section walls obey the Bohm Criterion, the flow to the walls is at the ion acoustic velocity. Ion escape rates to anode surfaces should be proportional to the product of the square-root of the local electron temperature and the plasma density. Because the plasma density near the anode in both the conical and the cylindrical section of the discharge chamber was determined to be approximately equal (ref. 10), the disparity between the ion wall flux measured at probe A and probe B must be due to the electron temperature. In this regard, the ratio between the two probes' current densities should be approximately equal to the ratio of the square root of the electron temperature measured at the two probes. Plots of these ratios as a function of discharge power are shown in figure 6. As can be seen from the plot, the average value of the ratio of the square root of the electron temperature is approximately 1.45, which within experimental error (10 to 15 percent) accounts for the difference in ion currents measured in the conical and cylindrical sections. This agreement supports the notion that a much higher percentage of ion production occurs just upstream of the ion optics and that the ion flow depends primarily on local plasma density and electron temperature. Because of the electron temperature disparity between the two discharge chamber sections, ion loss rates to the anode are largest in the cylindrical section, which in this case is just upstream of the optics. In this respect, ions are lost to the beam extraction optics at a rate larger than they are lost to anode surfaces in the conical section. Because ion losses to different sections of the discharge chamber are not uniform, the extracted ion fraction is not well represented by the ratio of screen grid open area to total discharge chamber surface area.

The nature of ion flow suggests the importance of understanding plasma conditions, particularly the local electron temperature and density, within the discharge chamber. Care must be taken such that the discharge is not only localized near the optics, but also that the ratio of the open area of the screen grid to the anode surface area near the optics is sufficiently large.

Electron Transport to Anode Surfaces between Magnetic Cusps

The discharge chamber magnetic field controls the flow of electrons to the anode. Ideally, in a ring cusp discharge chamber, most of the electron current collection occurs at the magnetic cusps. Under these conditions, the magnetic field between the cusps minimizes the flow of energetic electrons to other anode surfaces. In practice, depending on the field strength between the cusps, a significant fraction of the discharge current can be collected at the anode between the cusps. It was found in an earlier NSTAR- derivative thruster study that up to 30 percent of the discharge current can be collected at anode surfaces between the cusps (ref. 10). Because minimizing the flow of electrons to anode surfaces between the cusps improves thruster discharge efficiency, a understanding the nature of electron diffusion to anode surfaces between cusps is important.

In general the radial flow of electrons to the anode in the presence of a magnetic field may be expressed as (ref. 12):

$$J_e = -e \cdot \mu \cdot n_e \cdot E_s - e \cdot D_\perp \cdot \frac{dn_e}{dr} \tag{1}$$

Here mobility is defined as:

$$\mu = \frac{e}{m \cdot \nu_e} \tag{2}$$

Of interest is the functional behavior of the cross-field diffusion coefficient. In general, plasma flow across a magnetic field is a complicated problem. Under some conditions, plasma flow obeys classical formalism in which the cross-field diffusion coefficient can be described by:

$$D_\perp = \frac{D_e}{\left[1 + \left(\frac{\omega^2}{\nu_e^2}\right)\right]} \tag{3}$$

Here the electron diffusion coefficient under conditions where the magnetic field is zero is defined as:

$$D_e = \frac{k \cdot T_e}{m \cdot \nu_e} \tag{4}$$

Under certain conditions, potential oscillations driven by plasma instabilities give rise to anomalous cross-field diffusion that is substantially larger than classical predictions. In a variety of cases, such anomalous diffusion is best described by the Bohm diffusion coefficient (refs. 13 to 15):

$$D_\perp = \frac{kT_e}{16 \cdot e \cdot B} \tag{5}$$

In this work, using equation (1) and measured plasma properties, the electron current collected at and above plasma potential is calculated as a function of wall probe bias voltage. The total electron collision frequency, which is the sum of the electron-neutral collision frequency and the electron-ion collision frequency, was calculated based on ensemble averaged momentum exchange between the electrons and the background plasma using low energy electron-neutral and electron-ion cross section data (ref. 16 and 17). Neutral densities inside the discharge chamber were calculated from the propellant utilization efficiency. The calculation of the electron current is done assuming two separate cases: (1) Bohm diffusion and (2) Classical diffusion. The calculated electron current was then compared with the measured electron current to determine whether Bohm or classical best describes electron diffusion to anode surfaces between the magnetic cusps.

In order to calculate the electron current at the wall probes as a function of probe potential, the length scale for the potential and density gradients had to be first determined. The self consistency between the potential and the plasma density through Poisson's equation requires that the length scales of the potential and density gradient be

equal. The spatial extent of the gradient is assumed to include both the sheath and pre-sheath regions at the probe. To perform the calculation, equation (1) can be recast:

$$J_e = -e \cdot \mu \cdot n_{e_s} \cdot d \cdot \Delta V - e \cdot D_\perp \cdot \frac{n_e}{d} \qquad (1')$$

Here, $E_s = \Delta V \cdot d$, where ΔV is the potential difference between the probe and the plasma potential. The gradient thickness can be estimated from the slope of a plot of the measured electron current versus probe potential as defined in equation (1′). It is assumed that over the range of probe potentials investigated here, the gradient thickness, d, does not change appreciably with ΔV. As illustrated in figure 7, for all cases, the electron current as a function of probe voltage was linear. The constancy of the slope supports the assumption that the gradient thickness does not vary appreciably with increasing probe voltage over the voltage range investigated. From the slope, which was determined by linear curve fit, the effective gradient thickness, d, was determined. Gradient thickness at the 1.7 kW and the 2.3 kW condition at probe A were 2.1 and 2.4 mm, respectively, while at probe B, the thickness were 2.9 and 3.2 mm. It should be pointed out that the calculated gradient thickness, d, was approximately equal to the electron Larmor radius, the characteristic diffusion step for an electron in a magnetic plasma. This finding is not surprising in that electrons of sufficient energy that are located within a Larmor radius of the probe surface will be collected.

Using equation (1′), the electron current was calculated for both the Bohm diffusion coefficient and the classical cross-field diffusion coefficient. Figures 8 and 9 illustrate the behavior of the ratio of the calculated electron current to the measured electron current as a function of sheath voltage for the two wall probes at the 302 W discharge power condition (2.3 kW thruster input power) and at the 228 W discharge power condition (1.7 kW thruster input power). As can be seen from the figures, the electron collection between the cusps is best described by the classical cross-field diffusion coefficient. To within experimental error (~35 percent), the classical relation predicts the magnitude of the electron saturation current over a wide discharge power (200 to 465 W) range. Electron saturation current calculated assuming a Bohm diffusion coefficient was over an order of magnitude larger than that which was measured. Indeed, for the magnetic field intensities present between cusps, if cross-field diffusion were Bohm-like, then the utility of magnetic containment would be defeated due to excessive electron flow to anode surfaces between the cusps. It should also be pointed out that the classical relation for the electron current also tracked the functional behavior of the electron current with increasing probe voltage. The rate of change in the electron current with increasing probe voltage as calculated using the Bohm diffusion coefficient case was less than that actually measured as evidenced by the monotonically decreasing ratios presented in figures 8 and 9. Finally, it should be pointed out that the ratio of the electric field diffusion term to the magnetic field cross-diffusion term in equation (1) ranged from approximately 0.1 to 1 for classical diffusion with increasing probe voltage.

The fact that electron cross-field diffusion to intercusp anode surfaces is classical implies a number of interesting consequences: (1) Electron diffusion to the anode surface between cusps is severely reduced. (2) Operation at higher propellant flow rates should increase electron losses to the anode because of the classical diffusion coefficient's dependence on the electron collision frequency. (3) Modest increases in magnetic field strength should lead to significant improvements in electron containment.

Agreement between measured the electron current and the calculated classical current was best at the higher thruster power conditions (>1.4 kW). It should be pointed out that deviations from classical cross-field diffusion tended to increase at the lower power operating conditions. At these lower powers, the calculation for the electron current using the classical cross-field diffusion coefficient tended to under-estimate the measured value. The under-prediction trend at probe A ranged from 1 percent at the 2.3 kW input power condition to over 20 percent at the 1.4 kW input power. The discrepancy at wall probe B was somewhat larger than at probe A with the under-prediction trend ranging from 10 percent at the 2.3 kW input power condition to over 30 percent at the 1.4 kW input power.

Prior research suggests that deviations from the classical cross field diffusion may be due a plasma instability (refs. 12 and 18). Additionally, ionization along the flux lines between the cusps may become more important with decreasing discharge power. Drainage of inter-cusp flux lines via cross-field diffusion or a plasma instability would also tend to increase the magnitude of cross field current collected at the probe (ref. 19). These mechanisms may be necessary to sustain the magnitude of the discharge current at the lower thruster powers. The fact that measured electron diffusion to the anode between the magnetic cusps increases above the classical rate at the lower thruster power conditions suggests that electron containment between the cusps also degrades in concert. This degradation is consistent with the increased discharge losses at the lower power conditions. In this respect, characterization of electron diffusion phenomena to the anode is a key aspect for understanding discharge performance.

CONCLUSIONS

It was found that ion flow to anode surfaces just upstream of the ion optics is approximately equal to the average ion current density at the ion optics. Additionally, because ion losses to different sections of the discharge chamber are not uniform, the extracted ion fraction is not well represented by the ratio of screen grid open area to total discharge chamber surface area. Intercusp electron flow to the NSTAR-derivative ion thruster anode was found to follow classical diffusion predictions. This data suggests that modest increases in magnetic field intensity between the cusps can significantly improve electron containment.

REFERENCES

1. Kaufman, H.R., Robinson, R.S., and Frisa, L.A., "Ion Flow Experiments in a Multipole Discharge Chamber," *AIAA Journal*, vol. 22, no. 11, Nov. 1984, pp. 1544–1549.
2. Arakawa, Y. and Hamatani, C., "Reduction of Plasma Loss to Discharge Chamber Walls in a Ring-Cusp Ion Thruster," *J. Propulsion and Power*, vol. 3, no. 1, Jan.-Feb. 1987, pp. 90–91.
3. Sovey, J.S., "Improved ion containment using a ring-cusp ion thruster," *J. of Spacecraft and Rockets*, vol. 21, no. 5, May 1984, pp. 488–495.
4. Christensen, J.A., et al, "Design and Fabrication of a Flight Model 2.3 kW Ion Thruster for the Deep Space 1 Mission," AIAA Paper 98–3327, July 1998.
5. Kaufman, H.R. and Robinson, R.S., "Plasma Processes in Inert-Gas Thrusters," *J. Spacecraft and Rockets* vol. 18, no.5, Sept.-Oct. 1981, pp. 470–476.
6. Soulas, G.C., Foster, J.E., and Patterson, M.J., "Performance of Titanium Optics on a NASA 30 cm Ion Thruster," AIAA Paper 2000–3814, July 2000.
7. Sovey, J.S., et al, "Development of an Ion Thruster and Power Processor for New Millenium's Deep Space 1 Mission," AIAA paper 97–2778, December 1997.
8. Masek, T. D., "Plasma Properties and Performance of Mercury Ion Thrusters," *AIAA Journal*, vol. 9, no. 2, Feb. 1971, pp. 205–212.
9. Poeschel, R.L., "Development of Advanced Inert-Gas Ion Thrusters," NASA CR–168206, June 1983.
10. Foster, J.E., Soulas, G.C., and Patterson, M.J., "Plume and Discharge Measurements of an NSTAR-Type Ion Thruster," AIAA Paper 3812–2000, July 2000.
11. Brophy, J.R., "Simulated Ion Thruster Operation without Beam Extraction," AIAA Paper 90–2655, July 1990.
12. Chen, Francis, *Introduction to Plasma Physics and Controlled Fusion*, Plenum Press, NY, 1984, pp. 169–174.
13. Bohm, D., "Qualitative Description of the Arc Plasma in a Magnetic Field," *The Characteristics of Electrical Discharges in Magnetic Fields*, edited by A. Guthrie and R.K. Wakerling, McGraw-Hill Book Co., NY, 1949, pp. 1–12.
14. Chen, *Introduction to Plasma Physics and Controlled Fusion*, pp. 190–195.
15. Kaufman, H.R. and R.S. Robinson, *Operation of Broad Beam Ion Sources*, Commonwealth Scientific Corp., Alexandria, VA, 1984, pp. 143–144.
16. Frost, L.S., and A.V. Phelps, "Momentum-Transfer Cross Sections for Slow Electrons in He, Ar, Kr, and Xe from Transport Coefficients," *Physical Review*, vol. 136, no. 6 A, Dec. 1966, pp. 1538–1545.
17. Kaufman, *Operation of Broad Beam Ion Sources*, pp. 137–142.
18. Hoh, F.C. and Lehnert, B., "Diffusion Processes in a Plasma Column in a Longitudinal Magnetic Field," *Phys. Fluids*, vol. 3, no. 4, 1960, pp. 600–607.
19. Bernstein, I.B., Frieman, E.A., Kulsrud, R.M. and Rosenbluth, M.N., *Phys. Fluids*, vol. 3, no. 3, 1960, pp. 136–137.

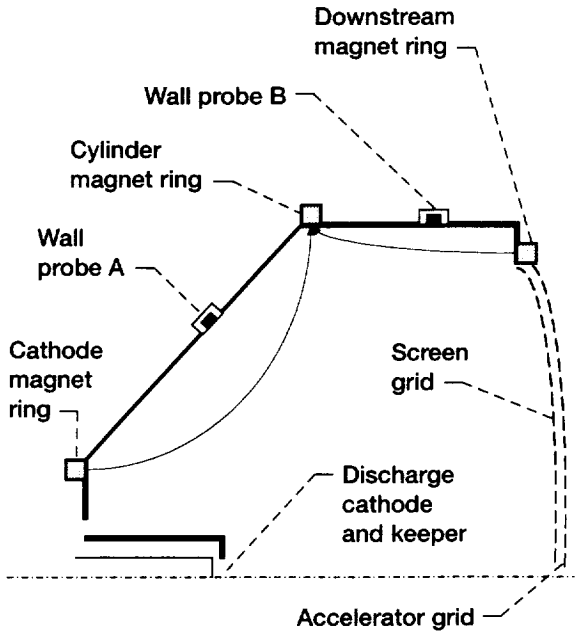

Figure 1.—Half-plane cross-section of NSTAR-derivative thruster revealing wall probes and magnetic circuit.

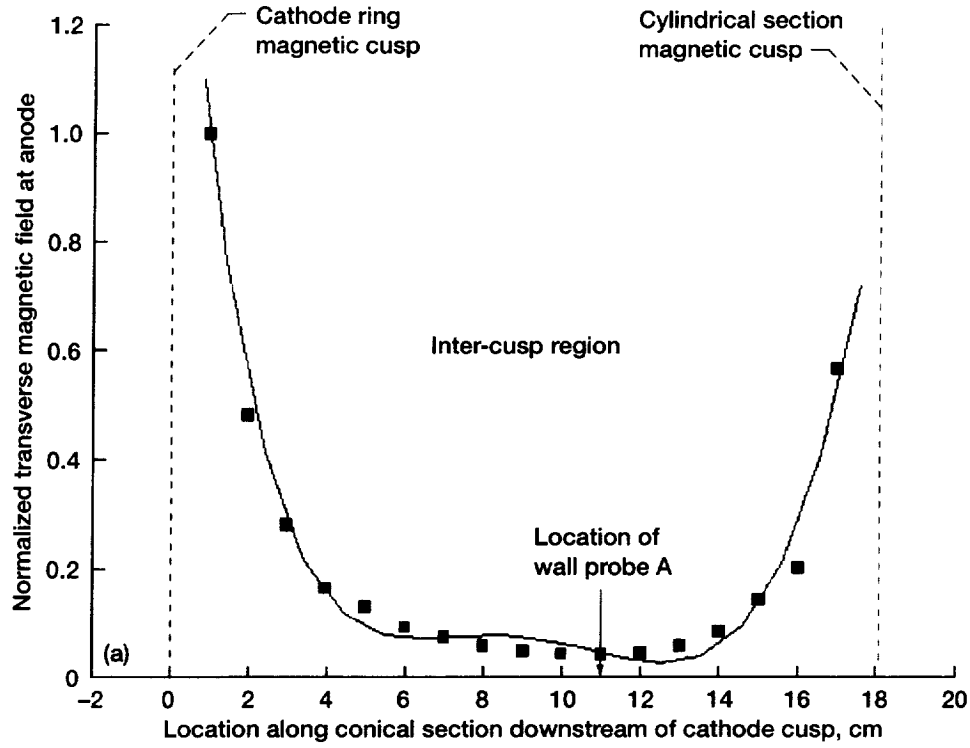

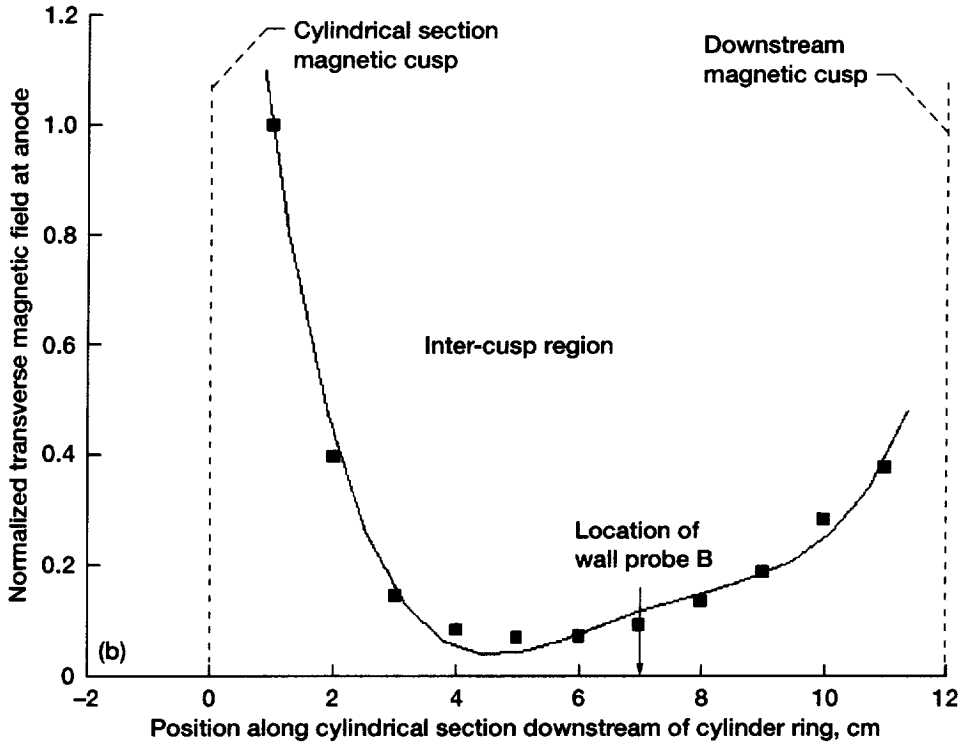

Figure 2(a).—Normalized transverse magnetic field between the cathode ring magnetic cusp and the cylindrical section magnetic cusp. This profile illustrates the transverse field behavior in the conical section of the discharge chamber. (b) Normalized transverse magnetic field between the cylindrical section magnetic cusp and the downstream magnetic cusp. This profile illustrates the transverse field behavior in the cylindrical section of the discharge chamber.

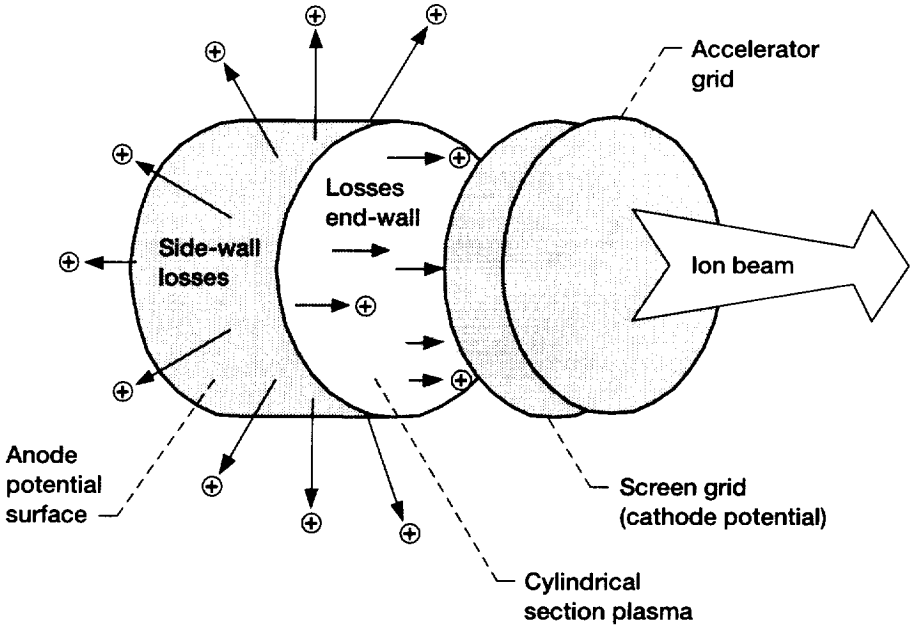

Figure 3.—Depiction of ion losses to the bounding discharge chamber anode surfaces and the ion optics.

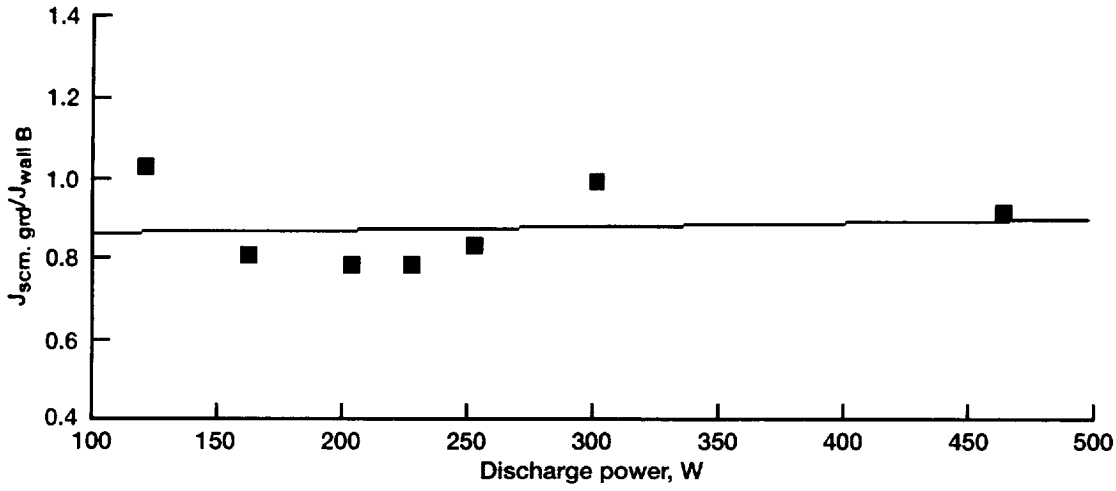

Figure 4.—Ratio of screen grid ion current density to ion current density measured at wall probe B as a thruster discharge power.

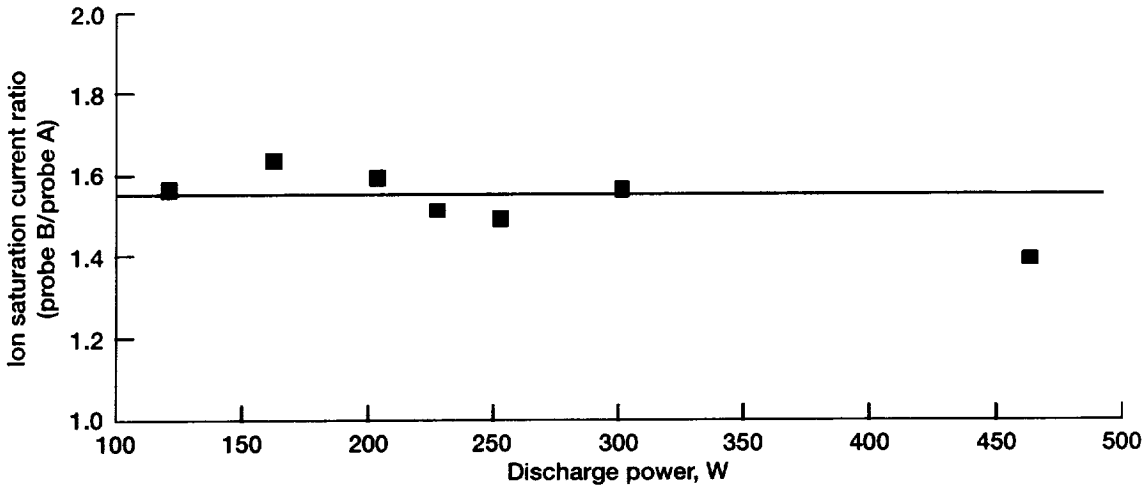

Figure 5.—Variations in the ratio ion saturation current measured at probe B to probe A as a function of discharge power.

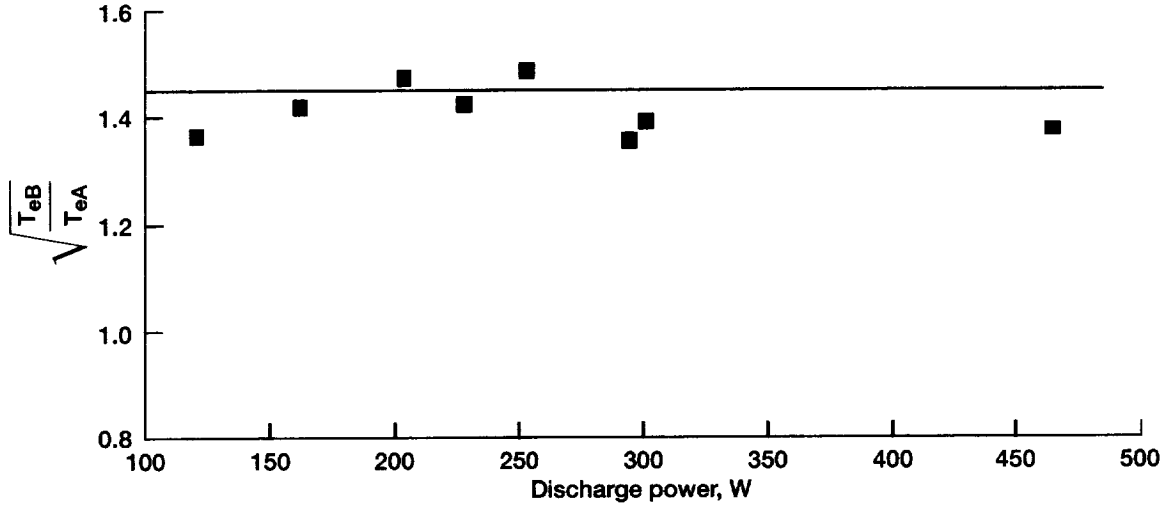

Figure 6.— Variations in the square-root of the electron temperature ratio of wall probe B to wall probe A.

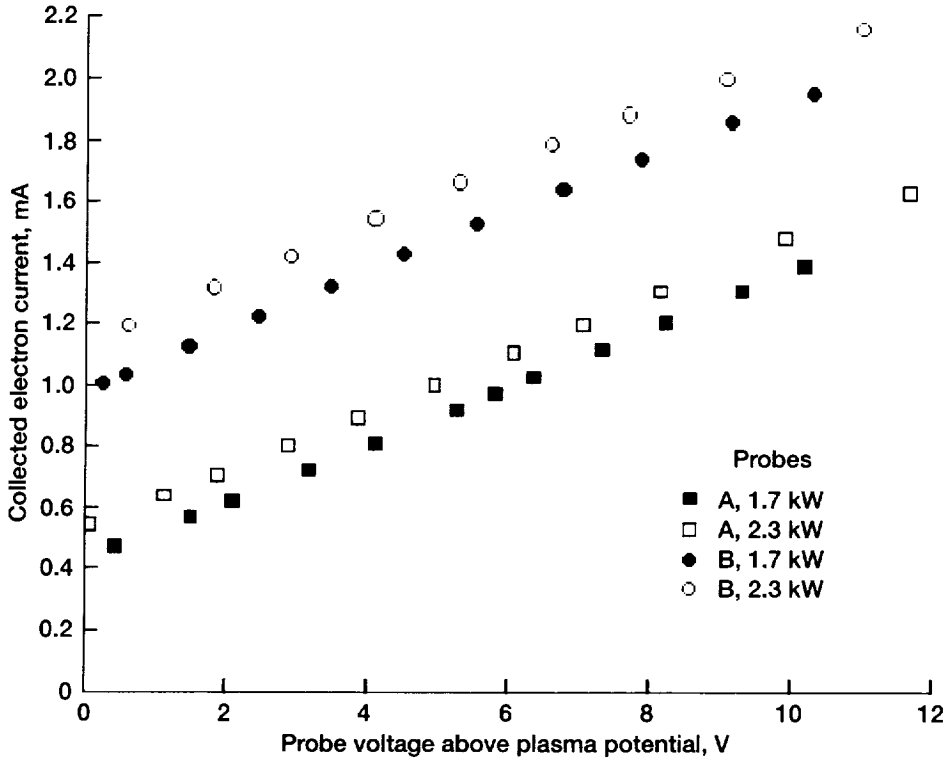

Figure 7.—Electron current collected at wall probes A and B as a function of probe voltage above the plasma potential.

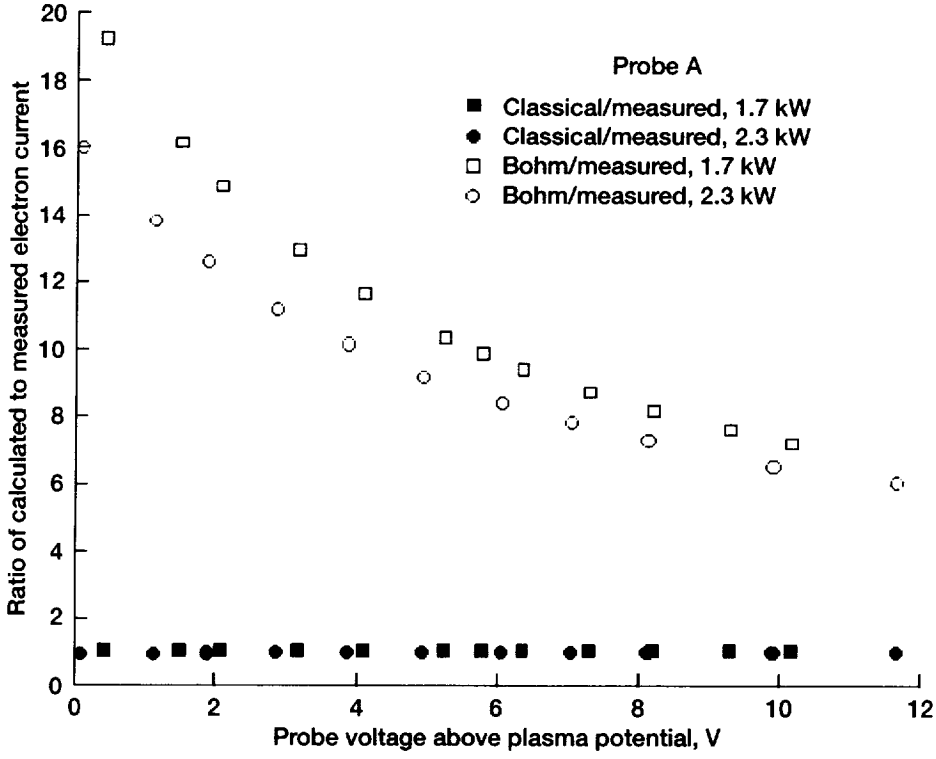

Figure 8.—Comparison between classical and Bohm electron flow to the anode between magnetic cusps at probe A (1.7 and 2.3 kW input thruster power).

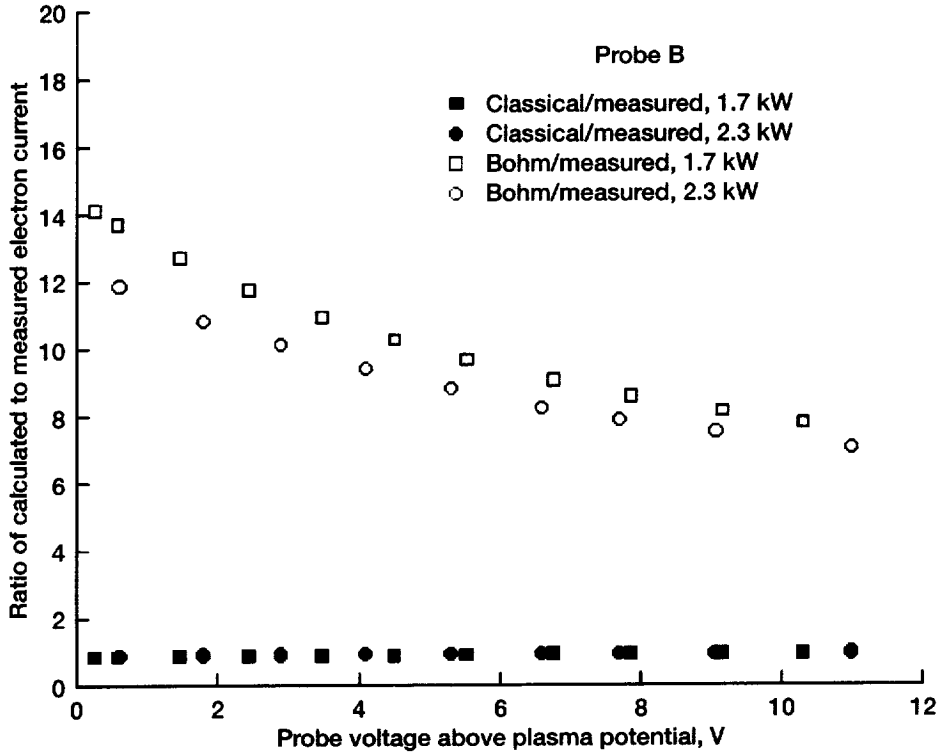

Figure 9.—Comparison between classical and Bohm electron flow to the anode between magnetic cusps at probe B (1.7 and 2.3 kW input thruster power).

REPORT DOCUMENTATION PAGE

Form Approved
OMB No. 0704-0188

Public reporting burden for this collection of information is estimated to average 1 hour per response, including the time for reviewing instructions, searching existing data sources, gathering and maintaining the data needed, and completing and reviewing the collection of information. Send comments regarding this burden estimate or any other aspect of this collection of information, including suggestions for reducing this burden, to Washington Headquarters Services, Directorate for Information Operations and Reports, 1215 Jefferson Davis Highway, Suite 1204, Arlington, VA 22202-4302, and to the Office of Management and Budget, Paperwork Reduction Project (0704-0188), Washington, DC 20503.

1. AGENCY USE ONLY (*Leave blank*)	2. REPORT DATE	3. REPORT TYPE AND DATES COVERED
	March 2001	Technical Memorandum

4. TITLE AND SUBTITLE

Inter-Cusp Ion and Electron Transport in a NSTAR-Derivative Ion Thruster

5. FUNDING NUMBERS

WU–632–6B–1B–00

6. AUTHOR(S)

John E. Foster

7. PERFORMING ORGANIZATION NAME(S) AND ADDRESS(ES)

National Aeronautics and Space Administration
John H. Glenn Research Center at Lewis Field
Cleveland, Ohio 44135–3191

8. PERFORMING ORGANIZATION REPORT NUMBER

E–12535

9. SPONSORING/MONITORING AGENCY NAME(S) AND ADDRESS(ES)

National Aeronautics and Space Administration
Washington, DC 20546–0001

10. SPONSORING/MONITORING AGENCY REPORT NUMBER

NASA TM—2001-210669

11. SUPPLEMENTARY NOTES

Responsible person, John E. Foster, organization code 5430, 216–433–6131.

12a. DISTRIBUTION/AVAILABILITY STATEMENT

Unclassified - Unlimited
Subject Categories: 75 and 20 Distribution: Nonstandard

Available electronically at http://gltrs.grc.nasa.gov/GLTRS
This publication is available from the NASA Center for AeroSpace Information, 301–621–0390.

12b. DISTRIBUTION CODE

13. ABSTRACT ***(Maximum 200 words)***

Diffusion of electrons and ions to anode surfaces between the magnetic cusps of a NASA Solar Electric Propulsion Technology Application Readiness ion thruster has been characterized. Ion flux measurements were made at the anode and at the screen grid electrode. The measurements indicated that the average ion current density at the anode and at the screen grid were approximately equal. Additionally, it was found that the electron flux to the anode between cusps is best described by the classical cross-field diffusion coefficient.

14. SUBJECT TERMS

Ion thruster; Magnetic field; Inter-cusp; Cross field diffusion; Electron diffusion; Anode

15. NUMBER OF PAGES

18

16. PRICE CODE

A03

17. SECURITY CLASSIFICATION OF REPORT	18. SECURITY CLASSIFICATION OF THIS PAGE	19. SECURITY CLASSIFICATION OF ABSTRACT	20. LIMITATION OF ABSTRACT
Unclassified	Unclassified	Unclassified	